



# Evaluation of Surface Crack Formation in Photovoltaic Backsheets Using Fragmentation and Finite Element Simulations

## Preprint

Stefan Mitterhofer,<sup>1</sup> Michael Kempe,<sup>2</sup> and Xiaohong Gu<sup>1</sup>

*1 National Institute of Standards and Technology*

*2 National Renewable Energy Laboratory*

*Presented at European Photovoltaic Solar Energy Conference and Exhibition 2023 (EU PVSEC)*

*Lisbon, Portugal*

*September 18-23, 2023*

**NREL is a national laboratory of the U.S. Department of Energy  
Office of Energy Efficiency & Renewable Energy  
Operated by the Alliance for Sustainable Energy, LLC**

This report is available at no cost from the National Renewable Energy Laboratory (NREL) at [www.nrel.gov/publications](http://www.nrel.gov/publications).

Contract No. DE-AC36-08GO28308

**Conference Paper**  
NREL/CP-5K00-85530  
October 2023



# Evaluation of Surface Crack Formation in Photovoltaic Backsheets Using Fragmentation and Finite Element Simulations

## Preprint

Stefan Mitterhofer,<sup>1</sup> Michael Kempe,<sup>2</sup> and Xiaohong Gu<sup>1</sup>

*1 National Institute of Standards and Technology*

*2 National Renewable Energy Laboratory*

### Suggested Citation

Mitterhofer, Stefan, Michael Kempe, and Xiaohong Gu2023. *Evaluation of Surface Crack Formation in Photovoltaic Backsheets Using Fragmentation and Finite Element Simulations: Preprint*. Golden, CO: National Renewable Energy Laboratory. NREL/CP-5K00-85530. <https://www.nrel.gov/docs/fy24osti/85530.pdf>.

**NREL is a national laboratory of the U.S. Department of Energy  
Office of Energy Efficiency & Renewable Energy  
Operated by the Alliance for Sustainable Energy, LLC**

This report is available at no cost from the National Renewable Energy Laboratory (NREL) at [www.nrel.gov/publications](http://www.nrel.gov/publications).

Contract No. DE-AC36-08GO28308

**Conference Paper**  
NREL/CP-5K00-85530  
October 2023

National Renewable Energy Laboratory  
15013 Denver West Parkway  
Golden, CO 80401  
303-275-3000 • [www.nrel.gov](http://www.nrel.gov)

## NOTICE

This work was authored in part by the National Renewable Energy Laboratory, operated by Alliance for Sustainable Energy, LLC, for the U.S. Department of Energy (DOE) under Contract No. DE-AC36-08GO28308. Funding provided by the U.S. Department of Energy Office of Energy Efficiency and Renewable Energy Solar Energy Technologies Office. The views expressed herein do not necessarily represent the views of the DOE or the U.S. Government. The U.S. Government retains and the publisher, by accepting the article for publication, acknowledges that the U.S. Government retains a nonexclusive, paid-up, irrevocable, worldwide license to publish or reproduce the published form of this work, or allow others to do so, for U.S. Government purposes.

This report is available at no cost from the National Renewable Energy Laboratory (NREL) at [www.nrel.gov/publications](http://www.nrel.gov/publications).

U.S. Department of Energy (DOE) reports produced after 1991 and a growing number of pre-1991 documents are available free via [www.OSTI.gov](http://www.OSTI.gov).

*Cover Photos by Dennis Schroeder: (clockwise, left to right) NREL 51934, NREL 45897, NREL 42160, NREL 45891, NREL 48097, NREL 46526.*

NREL prints on paper that contains recycled content.

# Evaluation of surface crack formation in photovoltaic backsheets using fragmentation and finite element simulations

Stefan Mitterhofer, Michael Kempe, Xiaohong Gu

**Abstract**—Backsheet cracking is among the most commonly observed degradation modes of photovoltaic (PV) modules in the field. Cracks can reduce the ability of backsheets to fulfil their functions, for example, protection of the modules from the environment or electrical insulation. This work presents an evaluation of the degradation and cracking propensity of two backsheets during accelerated IEC TS 62788-7-2 A3 (International Electrotechnical Commission) aging with the fragmentation test: a co-extruded polyamide backsheet (AAA), and a laminated multilayer backsheet with a polyethylene terephthalate core and outer layer and ethylene vinyl acetate inner layer (PPE). Results show the surface embrittlement of the AAA outer layer during exposure. A longer time of exposure causes cracks to form at lower strains during stretching and creates deeper cracks. Accordingly, Young’s modulus of the outer layer increases, as measured by cross-sectional nanoindentation. PPE exhibits cracking after exposure as well. While no similar increase of modulus or crack depth can be observed, the outer layer of PPE exhibits more obvious signs of erosion during exposure, including progressive morphological changes and thickness losses.

A finite element model to simulate surface crack formation is devised, based on initially zero-thickness decohesion elements. Decohesion criteria define a critical stress, at which these elements grow, and cracks can begin to form. These criteria are obtained via parameter optimization by comparison between simulation and experiment. The model is used to interpret crack formation in both backsheets.

**Index Terms**—backsheets, cracking, finite element method, photovoltaics, nanoindentation

## I. INTRODUCTION

The rapid growth of the photovoltaic (PV) market has made the technology an integral part of energy production in many countries, with further growth expected [1]. As such, its reliability and durability are becoming increasingly important. PV modules can be exposed to a wide variety of environmental stressors, for example elevated temperature, humidity and ultraviolet (UV) light, influencing several possible degradation mechanisms [2]–[4]. One of the most common module layouts consists of a front glass plate, cells and wiring potted in a polymer encapsulant, and a polymeric multi-layer backsheet, mounted together in an aluminum frame. The backsheet fulfills three crucial functions: (1) mechanical stability to the module,

making it more resistant to mechanical loading; (2) protection of the insides of the module from possibly harsh climatic conditions; and (3) protection to people from the high possible voltages and currents within the module. Backsheet cracking has been reported as one of the most common degradation modes observed in the field [5], [6]. It has been observed in many different materials, for example polyamide (PA) [7]–[10], polyvinylidene fluoride (PVDF) [11]–[13], and polyethylene terephthalate (PET), commonly in a multilayer with ethylene vinyl acetate (EVA) as a PET-PET-EVA (PPE) backsheet [13]–[15]. Such cracks can severely limit the backsheet’s ability to fulfill its functions. The degradation mechanisms and their dependence on the environmental parameters can thereby vary substantially depending on material selection. For example, PET is sensitive to hydrolysis, which can cause chain scission and embrittlement of the backsheet, leading to increased likelihood of crack formation [16]. On the other hand, PVDF has shown to become more brittle and exhibit more severe cracking in dry environments [11].

Material failures in many other applications have been connected to cracks [17]. In the first mathematical approach to evaluate a crack, Inglis examined a thin, infinite glass plate with an elliptical hole [18]. The stress at the tip of the major axis becomes infinite as the minor axis of the ellipse approaches zero. To evaluate crack propagation and material failure, Griffith applied a thermodynamical approach by examining the energy balance of the system with a crack and its change over time due to crack propagation [19]. However, the singularity at the crack tip remains an issue for the purpose of stress distribution calculations [17]. Numerical methods such as the finite element method (FEM) are nowadays used more often to evaluate cracks. However, the method has its drawbacks. It is not well suited for singular problems such as evaluation of a crack tip [20]. Possible approaches to alleviate these issues are adjusting the mesh density or using so-called singular elements in extended FEM (xFEM) [21], [22]. Furthermore, in general, adjacent finite elements are connected on their nodes, not enabling them to be split up. To implement the possibility of cracking in a material or delamination between two materials, initially zero-thickness interface elements have been developed, so-called decohesion elements [23], [24]. These elements

Stefan Mitterhofer (postdoctoral associate) is with the National Institute of Standards and Technology, Gaithersburg, MD 20899 USA (e-mail: [Stefan.Mitterhofer@nist.gov](mailto:Stefan.Mitterhofer@nist.gov)).

Michael Kempe is with the National Renewable Energy Laboratory, Golden, CO 80401, USA (e-mail: [Michael.Kempe@nrel.gov](mailto:Michael.Kempe@nrel.gov)).

Xiaohong Gu is with the National Institute of Standards and Technology, Gaithersburg, MD 20899 USA (e-mail: [Xiaohong.Gu@nist.gov](mailto:Xiaohong.Gu@nist.gov)).

enable the numerical evaluation of onsetting damage in materials.

FEM has been used extensively in PV to evaluate mechanical stresses within the modules at various steps of their lifetime, for example, during lamination, installation and in the field, and to correlate the results with possible degradation modes [25]–[28]. Some work is designed to better understand cracking in the electrically active parts of the modules, for example cells [29] and interconnects [30]. However, there is no model for backsheet cracking available in the literature yet. In this work, we propose a FEM model for backsheet surface cracking based on decohesion elements. Section II outlines the experiment, in which different backsheets are exposed to accelerated aging conditions and their crack propensity tested with the so-called fragmentation test [10], [14], [31], [32], as well as the simulation model. Section III presents both the measurement and simulation results, as well as a comparison between the two. Section IV presents a discussion and conclusion.

## II. METHODS

### A. Materials and Exposure

Two commercially available backsheets were used for this study. The first backsheet is a co-extruded PA based triple-layer backsheet (AAA). It is a backsheet with known cracking when used in field modules after a few years [7], [8]. The outer layer is  $(38 \pm 2) \mu\text{m}$ , the core layer  $(300 \pm 6) \mu\text{m}$  and the inner layer  $(28 \pm 2) \mu\text{m}$  thick. The second backsheet is a 7-layer laminated PPE, consisting of a PET outer layer, an adhesive, a PET core layer, another adhesive, and three EVA layers acting as an inner system. It is a common backsheet layout, which has also exhibited cracks in the field. The thicknesses of the respective layers are given in Fig. 1.

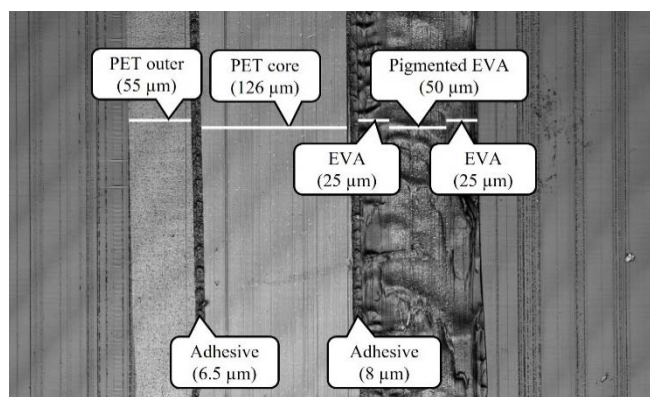


**Fig. 1.** LSCM image of the PPE backsheet cross-section showing its layout and thickness of each individual layer.

Several samples of both backsheets are degraded in an Atlas Ci5000 Weather-O-meter (Atlas Material Testing Technology, Mount Prospect, IL) under A3 conditions according to IEC 62788-7-2 [33], which consists of  $0.8 \text{ W/m}^2/\text{nm}$  at 340 nm,  $65^\circ\text{C}$  air temperature and 20 % RH, with a black panel temperature of  $90^\circ\text{C}$  using a filter combination compliant to ASTM D7869 [34].

### B. Backsheet characterization

After roughly 250 hours of exposure, a sample of each backsheet is extracted. They are potted in epoxy with the cross-section exposed and cut with a microtome (Leica Biosystems Nussloch GmbH, Nussloch, Germany). Young’s Modulus of each layer is evaluated with a G200 nano-indenter (KLA, Milpitas, CA) with a conical  $1 \mu\text{m}$  radius,  $60^\circ$  diamond tip. Additional measurements in the outer layer enable an in-depth evaluation of a possible depth-dependency of the modulus, which can be caused by degradation. The indents are then visualized under a Zeiss model LSM800 (Carl Zeiss Microscopy, White Plains, NY) laser scanning confocal microscope (LSCM), allowing accurate determination of their position. Further samples are cut into 5 mm wide strips for fragmentation testing. They are individually mounted into a mini-tensile tester and imaged through the 50x objective of the LSCM. Tensile testing is performed in a stepwise fashion increasing uniaxial strain on the sample, shown in Fig. 2. At each step, an image of a  $(715 \mu\text{m wide} \times 238) \mu\text{m}^2$  large area is taken, consisting of three  $(238 \times 238) \mu\text{m}^2$  squares. The number of visible cracks is counted to determine the surface crack density. To extract the crack depth, larger surface features are first removed and flattened out using a robust Gaussian filter according to the ISO (International Organization for Standardization) 16610-71 standard [35]. The average crack depth is extracted by evaluating two two-dimensional profiles across this area. To reduce the measurement noise, an integration over three areas normal to the direction of the applied strain is applied to these profiles, with each area being  $(155 \times 155) \text{ nm}^2$ . The maximum crack depth on the sample is extracted by searching for the largest pit depth according to the ISO 25178-607 standard [36].

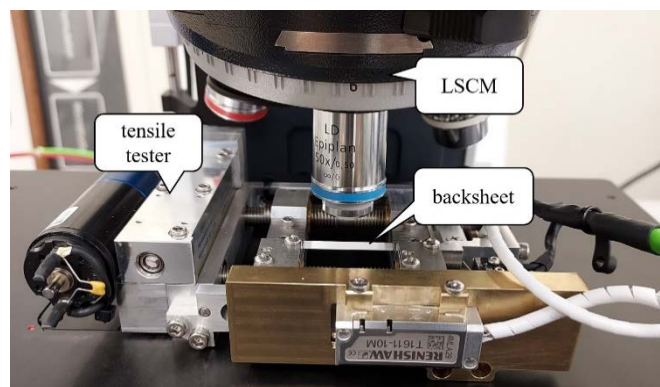


**Fig. 2.** Fragmentation setup with LSCM and mini-tensile tester

The characterization is repeated on all samples after 500 h, 1000 h, 1500 h, 2000 h, 3000 h, and 4000 h of exposure.

### C. Simulations

We create a finite element model for each backsheet, adding the properties of each layer. The exception are the EVA layers in PPE. They are simulated as one single layer instead of three distinct ones, because there were no measurable differences of the modulus between the EVA and the pigmented EVA layers.

Only elastic deformation is considered, outside of the cracks. The strain is added as a Dirichlet boundary condition on both sides of the backsheet in incremental steps. At each step, a stable solution to the time-independent problem is found.

We add several lines of initially zero-thickness decohesion elements [23] in regular intervals to define possible cracks in the outer layer. The distance between them is set to be in line with the saturation crack density measured in the corresponding fragmentation test. Because only surface crack formation was observed in the experiment, these lines only reach through the outer layer and do not penetrate further into the backsheet. Fig. 3 shows the mesh of the AAA backsheet.

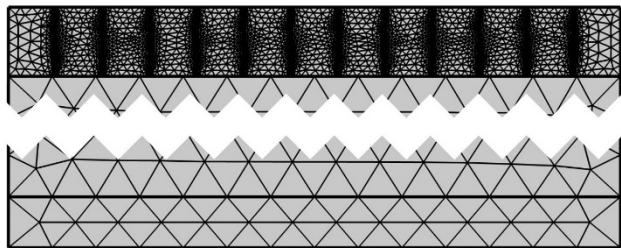


**Fig. 3.** Example simulation mesh for the AAA backsheet, with a possible crack density of up to 38 cracks/mm. The areas with the much finer mesh in the outer layer are adjacent to the decohesion elements.

A critical stress  $\sigma_{cr,i}$  is defined on each crack  $i$ . An adhesive force causes the decohesion elements to remain at zero thickness until  $\sigma_{cr,i}$  is met. This force is set in a way to not add additional stress or deformation of the material. In general, it can be a tensile stress, a shear stress, or a combination of both. Due to our experiment applying a tensile strain, we only focus on the tensile stress criterion, causing possible opening mode cracks (also called mode I cracks [17]). As soon as the decohesion criterium is fulfilled, the force is set to 0, which causes the decohesion elements to grow and a crack to form. Fig. 4 shows a schematic of this process.

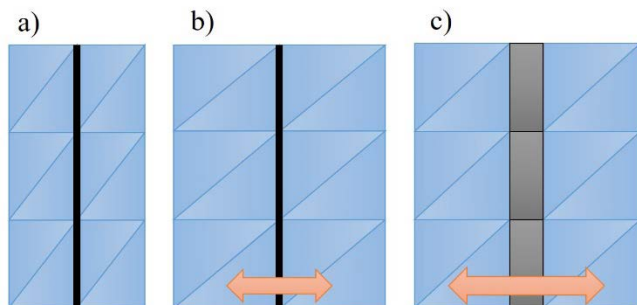


**Fig. 4.** a) Zero-thickness decohesion elements in the unstrained material. b) As the strain increases, the material deforms. However, while the decohesion criterium is not met, the decohesion elements remain at zero thickness. c) After the criterium is met, the decohesion elements grow and split the material, thus a crack begins to form.

Two experimental results are thereby important for the definition of  $\sigma_{cr,i}$ . The first result is the *crack depth*. We define

every  $\sigma_{cr,i}$  as a step function along the possible crack, where the position of the step is defined by the average crack depth obtained at 4 % strain. This value was chosen, because it is the maximum strain, at which crack propagation is limited to the outer layer in all samples. While such strains are realistic for fielded PV modules under normal operating conditions, localized maximal strains can also reach much higher values [37]. The decohesion criteria after the step position, i.e., further inside the material than the average crack depth, are set so high that it is not fulfilled even at the highest strains used in the experiment and simulations. The second important result is the *crack density* at different strains. As the polymer backsheet is not a perfectly homogeneous material, which does not degrade homogeneously, some cracks can form at different strains than others. We add this result in the simulations by varying  $\sigma_{cr,i}$  according to a three parameter Weibull distribution with the scale parameter  $k$ , shape parameter  $\lambda$  and offset  $\theta$ .

$$f(x, \lambda, k, \theta) = \begin{cases} \frac{k}{\lambda} \left( \frac{x - \theta}{\lambda} \right)^{k-1} \exp \left( - \left( \frac{x - \theta}{\lambda} \right)^k \right), & x - \theta \geq 0 \\ 0, & x - \theta < 0 \end{cases}$$

The random number generator (RNG) of MATLAB (MathWorks, Natick, MA) is thereby used to obtain the individual values of  $\sigma_{cr,i}$  according to the distribution. The parameters  $k$ ,  $\lambda$  and  $\theta$  are extracted with a parameter optimization using the Pattern Search algorithm. The target of the algorithm is the minimization of the root mean square error (RMSE) between each simulated strain in the simulations and a linear fit between the measurements at the closest two strains. For repeatability, the feed for the RNG is reset after each set of simulations. One set contains 10 simulations with 12 possible cracks each, where the leftmost and rightmost cracks of each simulation are excluded from this analysis. This step removes possible outliers on both sides of the backsheets in the simulations due to the edge. Each set thus consists of 100 possible cracks.

### III. RESULTS

#### A. AAA backsheet

##### A.1. Mechanical properties and surface morphology

The nanoindentation measurements on AAA show that the modulus of the outer layer increases after exposure, but not the core or the inner layer. The change in the outer layer is most pronounced on the exposed surface of the backsheet, seen in **Fig. 5**, with a larger depth affected after longer exposure. This result is in line with previous work on AAA degradation, due to an increase in crystallinity during accelerated aging of AAA. While photo-oxidation and corresponding chemocrystallization are primarily responsible for this increase, thermal processes can also accelerate these reactions [9], [10]. However, the surface morphology does not show any significant changes during exposure as observed under the 50x objective of the LSCM.

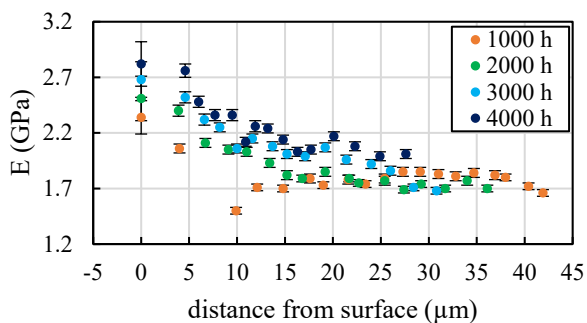


**Fig. 5.** Young’s modulus measured by nanoindentation in the AAA outer layer as a function of the distance to the surface. The measurement at 0 μm is taken on the outer layer surface, not in the cross-section sample. The error bars represent one standard deviation obtained from at least 40 indents for cross-sectional modulus measurements, and at least 15 indents for surface modulus measurements.

### A.2. Crack density and depth

No cracks can be observed during fragmentation of the fresh backsheet and of the 250 h-exposed sample. Fragmentation testing of the samples exposed 500 h or longer leads to cracking once a critical strain is applied. Additional strain causes, in general, further cracking until a saturation crack density is achieved. An example after 3000 h of exposure is shown in Fig. 6. At 1.4 % strain most cracks are already open, albeit very shallow and narrow. Further individual cracks form till 2.7 % applied strain. Increasing the strain further, the existing cracks grow wider, however, no new cracks are formed. Both critical strain and saturation crack density are thereby dependent on the time of exposure beforehand and, correspondingly, the degradation status of the backsheets’ outer layer. A longer exposure time correlates with a lower critical strain, i.e., cracks begin to form sooner during the fragmentation test. However, fewer cracks form, leading to a lower crack density, shown in Fig. 7. The error bars of measured crack densities in all corresponding figures show the standard deviation calculated from two or more cross-sections of a fragmentation measurement.

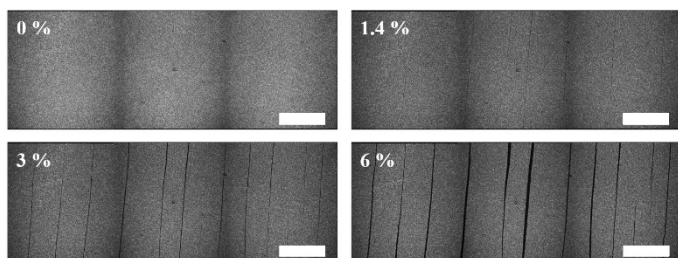


**Fig. 6.** LSCM images of 3000 h exposed AAA surface during fragmentation at various strains. The white scale bars indicate 100 μm length.

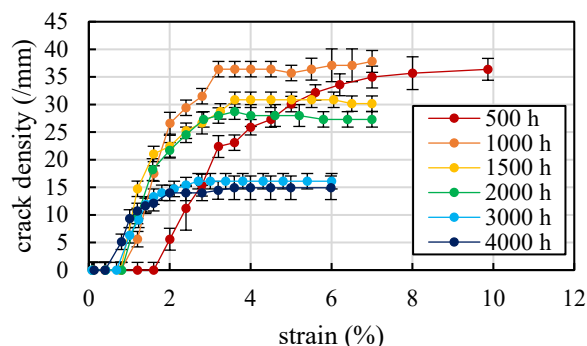


**Fig. 7.** Crack density as a function of strain in AAA after various exposure times. The standard deviation is calculated from at least two measurements on different areas of a sample.

A longer exposure time results in deeper cracks in strained samples. This result suggests, in combination with the modulus measurements, widening of a brittle region prone to cracking close to the exposed surface due to UV degradation. Increasing the strain causes further crack growth, shown in Fig. 8. It is limited to the outer layer, with one exception. After 4000 h of exposure, strains above 4 % cause several cracks to grow through the entire outer and into the core layer. The maximal crack depth at 4.5 % strain is  $(46.6 \pm 2.0) \mu\text{m}$ . The seemingly lower average crack depth at 6 % strain in this sample is caused by many thin cracks growing so deep, that not enough light is reflected out of them to be detected.

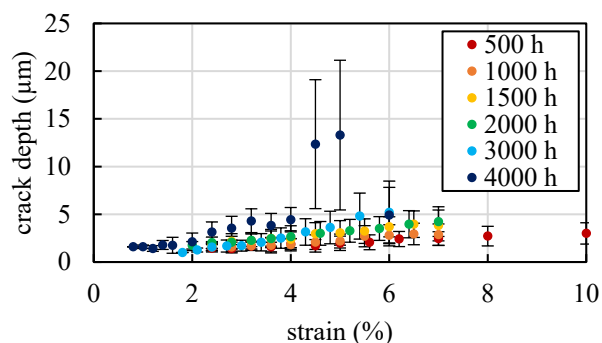


**Fig. 8.** Average crack depth in AAA samples after various times of exposure at increasing strain. The error bars show one standard deviation calculated from the depth of the visible cracks across two profiles.

## B. PPE backsheet

### B.1. Mechanical properties and surface morphology

Compared to the AAA backsheet, the change in modulus of the outer layer of the PPE backsheet after exposure is not significant. However, the loss in thickness and the increase in roughness are more pronounced for PPE as the exposure proceeds (Fig. 9 and Fig. 10), suggesting substantial degradation has occurred in the pigmented PPE outer layer. PET is known to be susceptible to photooxidation and chain scission during UV exposure, which can cause chemical and physical changes of a PET-based backsheet [14], [38]–[40]. The substantial thickness loss ( $\approx 16\%$ ) and roughness increase

( $\approx 500\%$ ) at 4000 h of exposure further indicates that the severe degradation of PET polymer can leave the surface dominated by the pigments, and the remaining products and pigments can be continuously depleted by erosion during exposure.

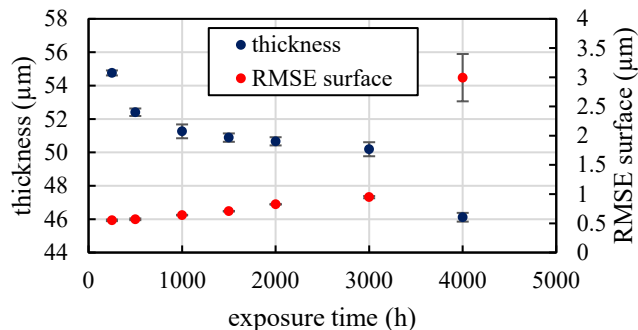


**Fig. 9.** Thickness of the PET outer layer as well as the RMSE of the outer layer surface height in PPE after different exposure times. The error bars of the thickness represent one standard deviation from 15 measurements, and the error bars of the surface RMSE represent one standard deviation from three measured locations.

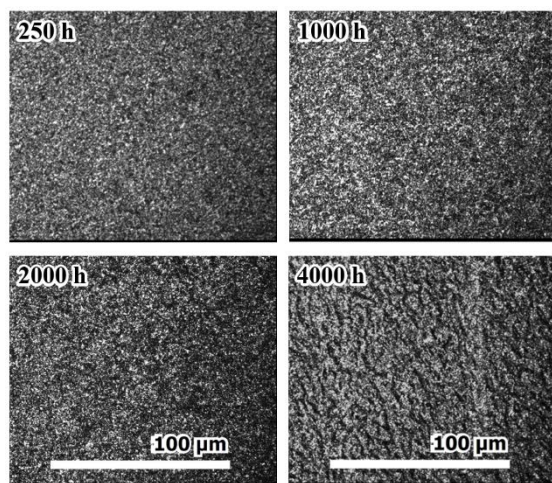


**Fig. 10.** LSCM images of the PPE outer layer surface after various times of exposure.

### B.2. Crack density and depth

Cracking behavior in PPE is similar to AAA, shown in Fig. 11. The fresh sample does not experience cracking. However, after 250 h of exposure, cracks begin to open after a critical strain is reached. Increasing the strain causes further cracks to open, until a saturation crack density is reached. However, some differences are observed between the two backsheets. At first, measurements after a longer exposure result in a decreased critical strain, the highest being observed in the shortest exposed sample. This trend reverses after 1000 h. A likely reason is the rougher surface due to degradation, which makes it more difficult to identify newly formed thin cracks. This effect is especially strong in the 3000 h and 4000 h exposed samples, which are impossible to evaluate using the LSCM, and are thus not included in this analysis.

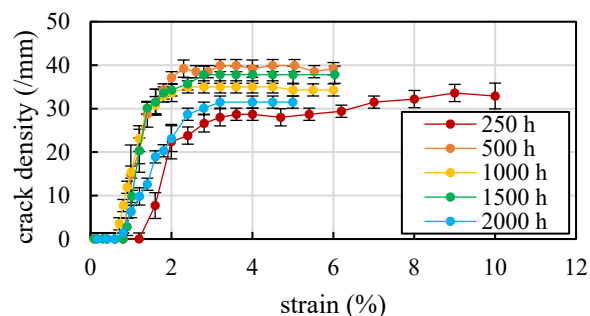


**Fig. 11.** Crack density as a function of strain in PPE after various exposure times.

The crack depth only slightly increases with a higher applied strain. Furthermore, there is no correlation between the time of exposure and crack depth, seen in Fig. 12. This behavior may be caused by the weathering and erosion of the outer layer, as the most strongly degraded parts are removed over time. The maximal measured crack depth is  $(8.6 \pm 1.0) \mu\text{m}$ , observed in the 500 h-exposed sample.

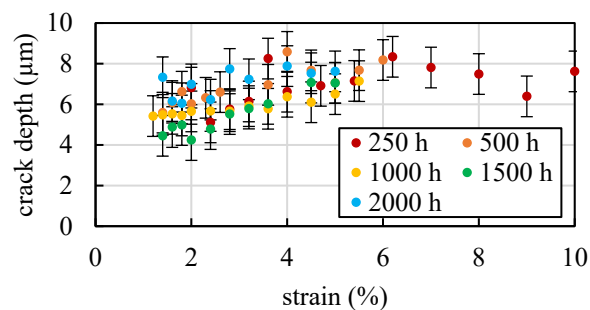


**Fig. 12.** Maximal crack depth in PPE after various times of exposure at different strain.

### C. FEM model parameter evaluation

Before looking at the comparison between FEM model and measurements, we evaluate the influence of different parameters on the simulation results. Varying the properties of core or inner layer has no effect on the results. This can be explained by the boundary conditions in the fragmentation experiment, where a certain strain is applied on the entire backsheet. In fielded PV modules, this strain depends on the properties of all layers of the entire module, such as thermal expansion coefficients or moduli [25]. Varying the properties of the outer layer influences the simulations. A higher modulus leads to cracks opening earlier, as the decohesion criteria are met at a lower strain, shown in Fig. 13. Increasing the crack depth while keeping the saturation crack density constant can reduce the crack density at certain strains, shown in Fig. 14. As a crack opens, the stress on its sides is reduced, shown by one example in Fig. 15. This crack density reduction affects a wider area for deeper crack, causing the decohesion criteria of nearby possible cracks to have a later onset.

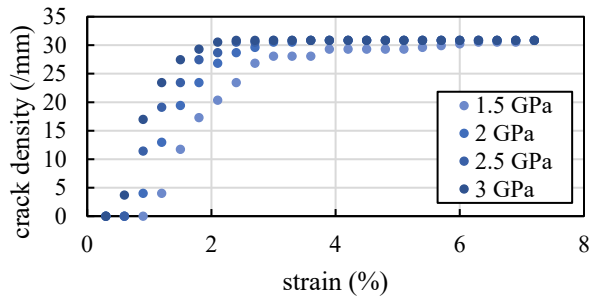


Fig. 13. Parameter variation of the modulus of the outer layer.

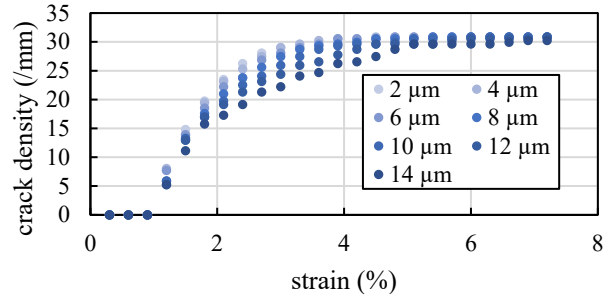


Fig. 14. Parameter variation of the crack depth.

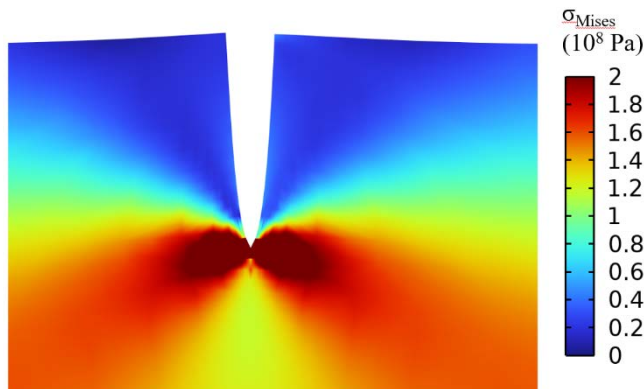


Fig. 15. Von Mises stress  $\sigma_{Mises}$  around a crack, with the visible singularity in the crack tip. The crack depth is  $14 \mu\text{m}$ .

#### D. Crack density simulations

The simulation model is, in general, able to fit the measured crack density in relation to applied strain with good accuracy and a low RMSE between experiment and simulation, shown by the example of AAA in Fig. 16 and by the example of PPE in Fig. 17. The corresponding parameters of the Weibull probability density functions are given in Table I, resulting in decohesion criteria in the unit of MPa. The optimized parameters are conclusive with the experimental results. In both backsheets, the initial increase in crack density with increasing strain is slower in the shortest exposed samples, seen in the higher  $k$ . In PPE both  $\lambda$  and  $\theta$  initially get smaller for longer exposed samples, indicating cracks formed at lower strains. However, the trend reverses after 1000 h of exposure as the PET outer layer surface degrades. While  $\lambda$  and  $\theta$  decrease after longer exposure in AAA, there is some larger variation of these parameters. Within certain limits both  $\lambda$  and  $\theta$  have a similar

effect on the RMSE, which can cause the optimization algorithm to find a good fit with one value higher and the other lower. Furthermore, the increased modulus of the outer polyamide layer in longer exposed samples can result in initial cracks being simulated at lower strains, causing an additional impact on the optimized  $\lambda$  and  $\theta$ .

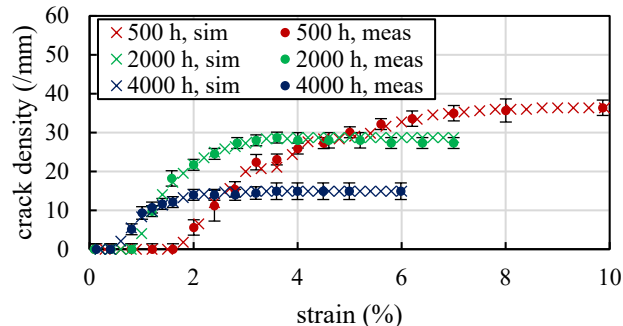


Fig. 16. Crack density in AAA in simulation and experiment.

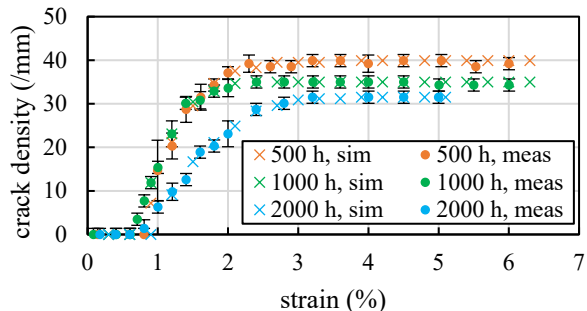


Fig. 17. Crack density in PPE in simulation and experiment.

TABLE I. OPTIMIZED WEIBULL PARAMETERS

Sample	$\lambda$	$k$	$\theta$	RMSE
AAA500	38.7	1.1	41	0.81
AAA1000	15	1	32.3	1.38
AAA1500	23.9	1	22.7	0.75
AAA2000	21	1	26.5	0.81
AAA3000	16.5	1	22.6	0.19
AAA4000	18.5	1	17.3	0.36
PPE250	45	1.1	55	2.81
PPE500	22.9	1	35	0.57
PPE1000	16.8	1	33	0.39
PPE1500	19	1	38.7	0.62
PPE2000	29	1	44	0.99

#### IV. DISCUSSION AND CONCLUSION

The fragmentation test has shown its capability of recreating backsheets cracking in a controlled environment for evaluating the cracking propensity of different backsheets after aging. AAA and PPE exhibit surface cracks, both reported in the field and in accelerated aging with subsequential fragmentation. Their cracking behaviors are, however, very different. Cracks in AAA reach deeper with longer exposure time as more severe degradation is observed. At a strain of  $\approx 4.5\%$ , the deepest cracks reached the core layer. Accelerated aging and field

results indicate that such cracks can eventually reach throughout the entire backsheet, leading to the backsheet failure[8], [9]. Outer layer cracks in PPE, on the other hand, were limited to a thin degraded region close to the surface. While surface and inner layer cracking are both reported for PPE in the field [13], [38], [41], there are no sources indicating these cracks propagate through the entire backsheets. Another factor for this behavior may be the very soft adhesives between the PET layers, and between the core PET and inner EVA layers. This adhesive layer can be much less prone to cracking due to their low modulus and can stop cracks propagating from one layer to the next. Coextruded backsheets such as AAA lack these soft adhesive layers, possibly making them more prone to crack propagation through multiple layers when core layers also experience severe degradation.

The finite element model was able to accurately recreate and interpret the measured crack density. The Weibull probability density functions of the decohesion criteria obtained by the parameter optimizations give an indication of the range of stress in the outer layer of the backsheet, at which cracks can happen. In the literature, simulations of the mechanical behavior of PV modules usually implement the backsheet as a single layer [25]. However, the properties of the individual layers can have a large impact on their cracking susceptibility, and thus should be included for a more complete analysis.

#### DISCLAIMER

Certain commercial products or equipment are described in this paper to specify adequately the procedure. In no case does such identification imply recommendation or endorsement by the National Institute of Standards and Technology, nor does it imply that it is necessarily the best available for the purpose.

#### REFERENCES

- [1] IEA (2022), "Solar PV," IEA, Paris. Accessed: Jun. 27, 2023. [Online]. Available: <https://www.iea.org/reports/solar-pv>
- [2] J. Ascencio-Vásquez, K. Brecl, and M. Topič, "Methodology of Köppen-Geiger-Photovoltaic climate classification and implications to worldwide mapping of PV system performance," *Sol. Energy*, vol. 191, pp. 672–685, Oct. 2019, doi: 10.1016/j.solener.2019.08.072.
- [3] D. C. Jordan, S. R. Kurtz, K. VanSant, and J. Newmiller, "Compendium of photovoltaic degradation rates: Photovoltaic degradation rates," *Prog. Photovolt. Res. Appl.*, vol. 24, no. 7, pp. 978–989, Jul. 2016, doi: 10.1002/pip.2744.
- [4] J. Kim, M. Rabelo, S. P. Padi, H. Yousuf, E.-C. Cho, and J. Yi, "A Review of the Degradation of Photovoltaic Modules for Life Expectancy," *Energies*, vol. 14, no. 14, p. 4278, Jul. 2021, doi: 10.3390/en14144278.
- [5] D. C. Jordan, T. J. Silverman, J. H. Wohlgemuth, S. R. Kurtz, and K. T. VanSant, "Photovoltaic failure and degradation modes: PV failure and degradation modes," *Prog. Photovolt. Res. Appl.*, vol. 25, no. 4, pp. 318–326, Apr. 2017, doi: 10.1002/pip.2866.
- [6] "DuPont global PV reliability - 2020 Field analysis," DuPont, 2020. Accessed: Jun. 27, 2023. [Online]. Available: <https://www.dupont.com/news/20200512-2020-global-pv-reliability-report.html>
- [7] Y. Lyu *et al.*, "Drivers for the cracking of multilayer polyamide-based backsheets in field photovoltaic modules: In-depth degradation mapping analysis," *Prog. Photovolt. Res. Appl.*, vol. 28, no. 7, pp. 704–716, Jul. 2020, doi: 10.1002/pip.3260.
- [8] G. C. Eder *et al.*, "Error analysis of aged modules with cracked polyamide backsheets," *Sol. Energy Mater. Sol. Cells*, vol. 203, p. 110194, Dec. 2019, doi: 10.1016/j.solmat.2019.110194.

- [9] S. Ulicna *et al.*, "Failure Analysis of a New Polyamide-Based Fluoropolymer-Free Backsheet After Combined-Accelerated Stress Testing," *IEEE J. Photovolt.*, vol. 11, no. 5, pp. 1197–1205, Sep. 2021, doi: 10.1109/JPHOTOV.2021.3090152.
- [10] Y. Lyu, J. H. Kim, A. Fairbrother, and X. Gu, "Degradation and Cracking Behavior of Polyamide-Based Backsheet Subjected to Sequential Fragmentation Test," *IEEE J. Photovolt.*, vol. 8, no. 6, pp. 1748–1753, Nov. 2018, doi: 10.1109/JPHOTOV.2018.2863789.
- [11] M. Owen-Bellini *et al.*, "Advancing reliability assessments of photovoltaic modules and materials using combined-accelerated stress testing," *Prog. Photovolt. Res. Appl.*, vol. 29, no. 1, pp. 64–82, Jan. 2021, doi: 10.1002/pip.3342.
- [12] S. L. Moffitt *et al.*, "Microstructure changes during failure of PVDF-based photovoltaic backsheets," *Prog. Photovolt. Res. Appl.*, vol. 31, no. 1, pp. 26–35, Jan. 2023, doi: 10.1002/pip.3605.
- [13] W. Gambogi *et al.*, "A Comparison of Key PV Backsheet and Module Performance from Fielded Module Exposures and Accelerated Tests," *IEEE J. Photovolt.*, vol. 4, no. 3, pp. 935–941, May 2014, doi: 10.1109/JPHOTOV.2014.2305472.
- [14] C.-C. Lin *et al.*, "Cracking and delamination behaviors of photovoltaic backsheets after accelerated laboratory weathering," presented at the SPIE Optics + Photonics for Sustainable Energy, N. G. Dhere, J. H. Wohlgemuth, and R. Jones-Albertus, Eds., San Diego, California, United States, Sep. 2015, p. 956304. doi: 10.1117/12.2188557.
- [15] A. Omazic *et al.*, "Relation between degradation of polymeric components in crystalline silicon PV module and climatic conditions: A literature review," *Sol. Energy Mater. Sol. Cells*, vol. 192, pp. 123–133, Apr. 2019, doi: 10.1016/j.solmat.2018.12.027.
- [16] G. Oreski and G. M. Wallner, "Aging mechanisms of polymeric films for PV encapsulation," *Sol. Energy*, vol. 79, no. 6, pp. 612–617, Dec. 2005, doi: 10.1016/j.solener.2005.02.008.
- [17] E. Gdoutos, *Fracture mechanics: an introduction*, Third edition. in Solid mechanics and its applications, no. volume 263. Cham: Springer, 2020.
- [18] C. E. Inglis, "Stresses in a plate due to the presence of cracks and sharp corners," *Trans. R. Inst. Nav. Archit.*, vol. 55, pp. 219–241, 1913.
- [19] A. A. Griffith, "VI. The phenomena of rupture and flow in solids," *Philos. Trans. R. Soc. Lond. Ser. Contain. Pap. Math. Phys. Character.* vol. 221, no. 582–593, pp. 163–198, Jan. 1921, doi: 10.1098/rsta.1921.0006.
- [20] T. Pin and T. H. H. Pian, "On the convergence of the finite element method for problems with singularity," *Int. J. Solids Struct.*, vol. 9, no. 3, pp. 313–321, Mar. 1973, doi: 10.1016/0020-7683(73)90082-6.
- [21] S. K. Chan, I. S. Tuba, and W. K. Wilson, "On the finite element method in linear fracture mechanics," *Eng. Fract. Mech.*, vol. 2, no. 1, pp. 1–17, Jul. 1970, doi: 10.1016/0013-7944(70)90026-3.
- [22] R. S. Barsoum, "On the use of isoparametric finite elements in linear fracture mechanics," *Int. J. Numer. Methods Eng.*, vol. 10, no. 1, pp. 25–37, 1976, doi: 10.1002/nme.1620100103.
- [23] P. P. Camanho, C. G. Davila, and M. F. De Moura, "Numerical Simulation of Mixed-Mode Progressive Delamination in Composite Materials," *J. Compos. Mater.*, vol. 37, no. 16, pp. 1415–1438, Aug. 2003, doi: 10.1177/0021998303034505.
- [24] D. Xie and S. B. Biggers, "Progressive crack growth analysis using interface element based on the virtual crack closure technique," *Finite Elem. Anal. Des.*, vol. 42, no. 11, pp. 977–984, Jul. 2006, doi: 10.1016/j.finel.2006.03.007.
- [25] P. Nivelle, J. A. Tsanakas, J. Poortmans, and M. Daenen, "Stress and strain within photovoltaic modules using the finite element method: A critical review," *Renew. Sustain. Energy Rev.*, vol. 145, p. 111022, Jul. 2021, doi: 10.1016/j.rser.2021.111022.
- [26] M. Haghi, M. Aßmus, K. Naumenko, and H. Altenbach, "Mechanical Models and Finite-Element Approaches for the Structural Analysis of Photovoltaic Composite Structures: a Comparative Study," *Mech. Compos. Mater.*, vol. 54, no. 4, pp. 415–430, Sep. 2018, doi: 10.1007/s11029-018-9752-6.
- [27] M. Owen-Bellini, D. Montiel-Chicharro, J. Zhu, T. R. Betts, and R. Gottschalg, "Influence of Viscoelastic Properties of Encapsulation Materials on the Thermomechanical Behavior of Photovoltaic Modules," *IEEE J. Photovolt.*, vol. 8, no. 1, pp. 183–188, Jan. 2018, doi: 10.1109/JPHOTOV.2017.2762583.
- [28] J. Y. Hartley *et al.*, "Effects of Photovoltaic Module Materials and Design on Module Deformation Under Load," *IEEE J. Photovolt.*, vol. 10, no. 3, pp. 838–843, May 2020, doi: 10.1109/JPHOTOV.2020.2971139.
- [29] N. Bosco, M. Springer, J. Liu, S. Nalin Venkat, and R. H. French, "Employing Weibull Analysis and Weakest Link Theory to Resolve Crystalline Silicon PV Cell Strength Between Bare Cells and Reduced-

- and Full-Sized Modules,” *IEEE J. Photovolt.*, vol. 11, no. 3, pp. 731–741, May 2021, doi: 10.1109/JPHOTOV.2021.3056673.
- [30] M. Springer, J. Hartley, and N. Bosco, “Multiscale Modeling of Shingled Cell Photovoltaic Modules for Reliability Assessment of Electrically Conductive Adhesive Cell Interconnects,” *IEEE J. Photovolt.*, vol. 11, no. 4, pp. 1040–1047, Jul. 2021, doi: 10.1109/JPHOTOV.2021.3066302.
- [31] J. H. Kim, Y. Lyu, A. Fairbrother, C.-A. Wang, and X. Gu, “An experimental approach to investigate behaviors of crack formation of PV backsheets,” in *2018 IEEE 7th World Conference on Photovoltaic Energy Conversion (WCPEC) (A Joint Conference of 45th IEEE PVSC, 28th PVSEC & 34th EU PVSEC)*, Waikoloa Village, HI: IEEE, Jun. 2018, pp. 1588–1592. doi: 10.1109/PVSC.2018.8547443.
- [32] M. D. Kempe, Y. Lyu, J. H. Kim, T. Felder, and X. Gu, “Fragmentation of photovoltaic backsheets after accelerated weathering exposure,” *Sol. Energy Mater. Sol. Cells*, vol. 226, p. 111044, Jul. 2021, doi: 10.1016/j.solmat.2021.111044.
- [33] IEC TC 82, “IEC TS 62788-7-2:2017 - Measurement procedures for materials used in photovoltaic modules - Part 7-2: Environmental exposures - Accelerated weathering tests of polymeric materials.” Sep. 06, 2017.
- [34] ASTM, “ASTM D7869-17 - Standard Practice for Xenon Arc Exposure Test with Enhanced Light and Water Exposure for Transportation Coatings.” Mar. 24, 2017.
- [35] ISO - International Organization for Standardization, “ISO 16610-71:2014 - Geometrical product specifications (GPS) - Filtration - Part 71: Robust areal filters: Gaussian regression filters.” Sep. 2019.
- [36] ISO, “ISO 25178-607:2019 - Geometrical product specifications (GPS) - Surface texture: Areal - Part 607: Nominal characteristics of non-contact (confocal microscopy) instruments.” Mar. 2019.
- [37] U. Eitner, “Thermomechanics of photovoltaic modules,” Martin-Luther-Universität Halle-Wittenberg, 2011. Accessed: Aug. 21, 2023. [Online]. Available: <https://opendata.uni-halle.de/handle/1981185920/7357>
- [38] A. Fairbrother *et al.*, “Degradation analysis of field-exposed photovoltaic modules with non-fluoropolymer-based backsheets,” in *Reliability of Photovoltaic Cells, Modules, Components, and Systems X*, M. D. Kempe, N. G. Dhere, and K. Sakurai, Eds., San Diego, United States: SPIE, Aug. 2017, p. 2. doi: 10.1117/12.2272488.
- [39] X. Gu, L.-C. Yu, Y. Lyu, J. H. Kim, A. Fairbrother, and T. Nguyen, “Impact of UV Light Intensity on Photodegradation of PV Backsheets,” in *2017 IEEE 44th Photovoltaic Specialist Conference (PVSC)*, Washington, DC: IEEE, Jun. 2017, pp. 3204–3207. doi: 10.1109/PVSC.2017.8366756.
- [40] X. Gu *et al.*, “Wavelength Sensitivity in Photodegradation of Polymer PV Backsheets,” in *2018 IEEE 7th World Conference on Photovoltaic Energy Conversion (WCPEC) (A Joint Conference of 45th IEEE PVSC, 28th PVSEC & 34th EU PVSEC)*, Waikoloa Village, HI: IEEE, Jun. 2018, pp. 1583–1587. doi: 10.1109/PVSC.2018.8547730.
- [41] M. D. Kempe, T. Lockman, and J. Morse, “Development of Testing Methods to Predict Cracking in Photovoltaic Backsheets,” in *2019 IEEE 46th Photovoltaic Specialists Conference (PVSC)*, Chicago, IL, USA: IEEE, Jun. 2019, pp. 2411–2416. doi: 10.1109/PVSC40753.2019.8980818.